OPEN ACCESS

Water-circulating probes significantly modify lesion length and axon damage in cooled radiofrequency ablations when compared with similar-sized standard radiofrequency probes in rats

Alyssa Cobbs ,[1] Guillermo Alas,[1] Ruchi Yadav,[1] Jacques Mayeux,[1] Maxim S Eckmann,[2] David Anthony Provenzano ,[3] Arthur W English,[4] Alencia Washington,[1] Ruoya Wang[1]

► Additional supplemental material is published online only. To view, please visit the journal online (http://dx.doi.org/10.1136/rapm-2023-104554).

[1]Research and Development, Avanos Medical Inc, Alpharetta, Georgia, USA
[2]Anesthesiology, Univ Texas Hlth Sci Ctr San Antonio, San Antonio, Texas, USA
[3]Pain Diagnostics and Interventional Care, Sewickley, Pennsylvania, USA
[4]Cell Biology, Emory University, Atlanta, Georgia, USA

Correspondence to
Dr Alyssa Cobbs;
alyssa.cobbs@avanos.com

Received 4 April 2023
Accepted 14 August 2023
Published Online First
24 September 2023

ABSTRACT

Introduction Preclinical research demonstrated water-cooled radiofrequency (CRF) ablations have a significant impact on structural and functional changes compared to standard radiofrequency (SRF) ablations. Clinical procedures utilizing RF to treat chronic pain conditions also show sustained functional outcomes. We hypothesize that the design of the RF probes plays an important role in interventional procedure success, but it remains unclear which specific design features.

Methods RF ablations were performed in male Lewis rats (n=51) using multiple-sized probes for CRF (17 Ga/2 mm and 17Ga/4 mm) and SRF (22Ga/5 mm, 18Ga/10 mm and 16Ga/10 mm) to evaluate generator energy output, lesion length, axon damage by histology and nerve function analysis via electromyography. To exclude probe design variables beyond size and remain objective, we tested cooled probes with and without water circulation, which resulted in the CRF probe performing like an SRF probe.

Results Consistent with our previous findings in smaller probes, CRF large probes delivered more energy ($p<0.01$) and generated multiple zones of thermal damage in sciatic nerves. When the water-circulating feature was turned off, however, energy output ($p<0.001$) and lesion length ($p<0.05$) was significantly reduced. CRF probes with the water circulation also featured significantly more axonal disruption, than larger sized SRF probes ($p<0.0001$).

Conclusions Overall, this data confirms that CRF's water-circulating technology has a greater impact on energy deposition, lesion length and axon damage compared with SRF ablations. Moreover, results suggest that the structural differences between RF modalities cannot be solely attributed to probe size, and it may shed light on its differences in clinical outcomes.

WHAT IS ALREADY KNOWN ON THIS TOPIC

⇒ A head-to-head comparison of two radiofrequency ablation (RF) systems indicated cooled radiofrequency (CRF) ablations produce greater energy output and more significant changes to peripheral nerves compared to standard radiofrequency (SRF) ablations.

⇒ However, literature suggests that RF probe design modifications can influence lesions and previous studies were limited in the use of more clinically common probe sizes.

WHAT THIS STUDY ADDS

⇒ We highlighted the impact of CRF's water-circulating probe design, resulting in significant changes in lesion characteristics, rather than probe size alone.

HOW THIS STUDY MIGHT AFFECT RESEARCH, PRACTICE OR POLICY

⇒ This study reveals the importance of design features beyond probe size for RF-desired tissue damage.

⇒ Therefore, clinicians should consider probe design features in addition to probe size when selecting the appropriate generator and probe configurations for ideal interventional success.

INTRODUCTION

Radiofrequency ablation (RFA) is an established treatment for back pain and peripheral joint pain.[1–4] RFA is a minimally invasive therapy that generates thermal damage, known as lesions, to impair pain signals in sensory nerves.[5] In previous research, several probe configurations and generator settings were compared with assess RFA lesion shape.[6] Cosman *et al* observed that standard radiofrequency (SRF) probes have a sharp and beveled active tip, which creates ellipsoid lesions. In contrast, cooled radiofrequency (CRF) probes have a blunted active tip and an internal water circulation system throughout the probe, which creates spherically shaped lesions.

The electrode–tissue interface of probe designs can also have varying effects on the formation of lesions.[7 8] According to Haines *et al*, extended periods of ionic heating at the SRF probe tissue–interface can lead to tissue charring, which limits lesion size by preventing subsequent energy movement beyond desiccated tissue. In contrast, the CRF probe's water circulation system allows lower temperatures at the electrode–tissue interface,

To cite: Cobbs A, Alas G, Yadav R, *et al*. *Reg Anesth Pain Med* 2024;**49**:448–454.

resulting in larger lesions being formed because energy is delivered to adjacent tissues without creating desiccation. Literature suggests that RF probe design modifications, such as tip gauge, length and tissue contact, can heavily influence the size and shape of resulting lesions.

Studies in ex vivo and preclinical models have shown that CRF probes produce significantly larger lesion volumes compared to SRF probes.[9 10] While there have not been any large, prospective, randomized trials comparing the two in clinical practice, literature on genicular nerve ablations has confirmed extended clinical durability for SRF up to 12 months[11–13] and CRF up to 24 months.[14–16] These studies suggest that lesion size and the amount of energy delivered to a target nerve may impact clinical durability. Therefore, it is important for clinicians to understand the factors that influence RFA lesion size and shape, so they can select the appropriate generator and probe configurations for ideal interventional success and desired tissue damage.

In a study conducted by Zachariah *et al*, CRF ablations produced greater energy output and more significant changes to peripheral nerves compared to SRF ablations.[10] However, the use of larger SRF probes to achieve equivalent lesion size and thermal damage is still under debate. Therefore, to investigate the impact of probe size on structural and functional outcomes in a rodent sciatic nerve (SN) model, we utilized clinically common probe sizes for both RF technologies. We hypothesize that CRF's water-circulating probe feature, not probe size alone, is the primary driver of greater energy output, leading to larger lesions and more axonal disruption than SRF probe ablations.

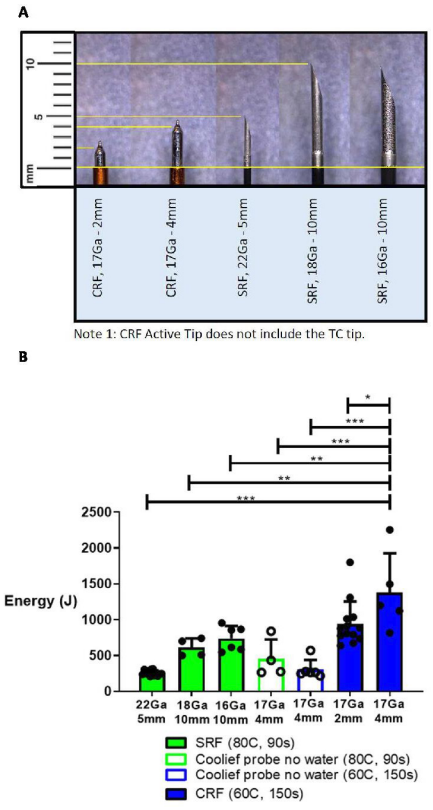

Figure 1 Cooled RF probes delivered more energy than any size standard RF probes at RF clinic parameters. (A) Cooled and standard probe sizes (gauge/active tip length). (B) Generator power output data were collected from SRF or CRF ablations to calculate energy (in joules, J) at 90 s and 150 s, respectively. 'Cooled probe with no water' denotes a cooled probe delivering RF energy without the water circulation through the probe. Bars represent mean±SD for n=4–13 per group per treatment. Statistical significance was indicated as *P<0.05, **P<0.01, ***P<0.001. CRF, cooled radiofrequency; SRF, standard radiofrequency; TC, thermacouple.

METHODS

Animal surgical and radiofrequency procedures

All studies included male Lewis rats between 250 and 300 g. Animals were kept on a 12-hour light/dark schedule and fed on an ad libitum basis. Animals were subjected to anesthesia to perform surgical SN exposure for probe placement and radiofrequency ablations or sham operation (control), as previously described.[10] Animals were anesthetized either using 1%–2% isoflurane or a combination of ketamine (150 mg/kg) and xylazine (9.6 mg/kg). Buprenorphine was administered for post-procedural pain relief. Following sciatic nerve exposure, either an SRF cannula (22Ga, 100 mm long, 5 mm active tip—PMF-22-100-5) (18Ga, 100 mm long, 10 mm active tip—PMF-18-100-10) (16-Ga, 100 mm long, 10 mm active tip—PMF-16-100-10) or CRF introducer (17Ga, 75 mm long, 2 mm active tip—CRI-17-75-2) (17Ga, 75 mm long, 4 mm active tip—CRI-17-75-2) from Avanos Medical (Alpharetta, Georgia) was inserted through the skin, distal to the nerve. Following the stylet removal, the respective SRF and CRF probes (PMP-22-100-5, PMP-18-100-10, PMP-16-100-10 SRFA and CRP-17-75-2, CRP-17-75-4 CRFA, Avanos Medical) (figure 1A) were positioned directly under the SN for SRF and CRF procedures using visual guidance. Probe sizes were chosen to include a variety of comparatively similar, commonly used and commercially available sizes. The RF generator was set to auto-temp mode to start the ablation and began when the impedance values fell within the expected range (150–200 Ω) from the generator (PMG-Advanced, Avanos Medical).

The first cohort of animals (n=41) utilized RFA procedure parameters commonly used in human clinical settings. For SRF groups, the generator temperature was set at 80°C for a run duration of 90 s using 22Ga, 5 mm (n=13), 18Ga, 10 mm (n=4) and 16Ga, 10 mm (n=6) probe sizes. The CRF groups were set at 60°C for 150 s using 17Ga, 2 mm (n=13) and 17Ga, 4 mm (n=5) probe sizes. To isolate water as a variable in RFA energy output, additional animal groups described as 'Cooled probe, No water' used CRF probes 17Ga/4 mm with the probe tip water-circulating feature turned off. Cooled probes without water were run at SRF parameters (n=4) and CRF parameters (n=6), as discussed, to evaluate the effect of time and temperature variables when the interaction of fluids during the procedure was eliminated.

From cohort 1, a subset of animals were treated with comparable large probes (SRF 16Ga/10 mm, SRF 18Ga/10 mm or CRF 17Ga/4 mm) and further evaluated via electromyography (EMG) or blinded histological assessment within 6 hours following the RF ablations.

Generator power output recording and energy calculations

A laptop computer connected to the RF generator recorded the generator power output every 0.2 s. The total energy in joules (J) was calculated by integrating the total power delivered across the total run duration, for each SRF or CRF run. SRF and CRF run durations were based on times typically used in the clinic, as described above.

Electromyography

EMG experiments were performed before and immediately following the sham or RF procedure. A sham RF procedure

was performed in one group and three groups received RF ablations of the SN, using either an SRF probe (18Ga/10 mm and 16Ga/10 mm) or a CRF probe (CRFA 17Ga-4mm). The animals were anesthetized during EMG recordings. For all such recordings, before and after the ablation bipolar fine wire EMG electrodes (California Fine Wire Company, Grover Beach, California; Stablohm 800 A, material number cfw-100189) were inserted into the gastrocnemius muscle (GAST) via 25Ga hypodermic needle. The position of wire electrodes was in similar locations in the muscles during each trial in every animal to maintain consistency. EMG activity was amplified (X1000) and recorded from these electrodes in response to constant voltage electrical stimulation of the SN with 0.3 ms pulses. Compound muscle action potentials (short-latency direct muscle responses or M-responses) were recorded from the GAST muscles using custom Labview software and recorded to disc. During recordings, stimulus intensity was increased gradually until an M response of maximal amplitude (Mmax) was observed. Stimuli were delivered, no more than once every three seconds to reduce the possibility of fatigue. The duration, amplitude and latency of Mmax were measured from the evoked responses, as previously described.[17 18]

Histological analyses

To study early post-injurious outcomes of thermal lesions including any evidence of secondary injury or cellular responses induced by SRF and CRF ablations, SNs were collected within 6 hours following the treatment. These time points were acquired from a previously published review by Choi *et al*,[19] indicating neural regeneration after neural ablation may begin as early as 30 min post-injury. Animals were euthanized via intracardiac injection of pentobarbital sodium and phenytoin sodium solution (2 mEq/kg) with an isoflurane plane of anesthesia. SNs were then extracted and postfixed in 10% formalin, embedded in paraffin and sectioned. One cohort of rat SNs was harvested immediately postablation, sectioned longitudinally (along the length of the nerve) into 5 µm-thick sections, and lesion measurements were assessed. The total length of the lesioned SN was captured on each slide and was measured (in mm). To compare the true effect of probe size between technologies, lesion size was expressed as a proportion of active tip length. The ablation zone was defined as the region of coagulated collagen and/or acute necrosis (including a central cooled zone, if present), as previously described.[10]

The second cohort of rat SNs was collected immediately after and 6 hours postablation. Following the collection, nerves were processed and embedded to create two cross-sections (proximal and distal segments). Nerves were embedded such that the superficial block contained the central portion of the nerve and were sectioned into 4 µm-thick sections to span the lesioned area. SN samples were H&E-stained and the degree of thermal damage was scored by an independent histopathologist (Histotox Labs, Boulder, Colorado). Lesion measurements were performed on whole slide images and measured in millimeter (mm). To evaluate the extent and severity of each lesion, the thermal injury zones were graded as follows and were scored 0–5, where 0=absent, 1=minimal, 2=mild, 3=moderate, 4=marked, 5=severe. Axon swelling and axon separation, the distance between the boarders of axon sheaths, were measured at five random sites within the nerve fascicles and the average (mean sum) was calculated.

Immunohistochemistry

For immunohistochemistry (IHC) staining in cross-sectioned rat SN, staining was conducted on a Leica Bond RXm platform using standard chromogenic methods. Glass slides were evaluated by a board-certified veterinary pathologist using light microscopy.

All antibodies were developed in rabbit (Abcam, Waltham, Massachusetts). 3% H2O2 was used to block endogenous peroxidases and 1% casein was used to block non-specific protein binding. For antigen retrieval, slides were incubated with proteinase K for 5 min at room temperature neurofilament heavy chain (NEFH, axons) (dilution: 1:400), heated in a pH6 Tris-based buffer for 2 hours at 70°C for myelin basic protein (MBP) (dilution: 1:500) and S100α (Schwann cells) (dilution: 1:100), heated in a pH9 EDTA-based buffer for 2 hours at 70°C for CD11b (inflammatory cells) (dilution: 1:10,000), or heated in a pH9 EDTA-based buffer for 25 min at 94°C for Myelin proteolipid protein (PLP) (dilution: 1:100), followed by followed by a 30 min, ambient temperature antibody incubation. Antibody binding was detected using an HRP-conjugated, antirabbit secondary polymer, followed by chromogenic visualization with diaminobenzidine. A hematoxylin counterstain was used to visualize nuclei.

Findings from the IHC staining in this study were generally qualitative due to morphological changes induced by RF ablations. Mean scores were used to evaluate the relative abundance of staining in each nerve section. Findings were scored 0–5, where 0=none (0%); 1=minimal (1%–10%), 2=mild (11%–25%), 3=moderate (26%–50%), 4=marked (51%–75%) and 5=severe (>75%).

Statistical analysis

Statistical analysis was performed using GraphPad Prism V.5.0 statistical software (Graphpad Software, La Jolla, California) using either a one-way or two-way analysis of variance to compare the means of multiple treatment groups. All quantitative data are expressed as mean±SD and are noted as such under each figure. Post hoc tests for multiple comparisons were used where appropriate. Statistical significance was set at $p<0.05$.

RESULTS

CRF probes delivered more energy than any size SRF probe

The mean energy (mean±SD) delivered by the RF generator at the clinical treatment parameters increased as probe size increased for CRF (60°C for 150 s) and SRF (80°C for 90 s) ablations independently (figure 1B). When comparing the RF technologies head-to-head, 17Ga/2 mm and 17Ga/4 mm CRF probes delivered significantly more energy than all SRF probe sizes, 943.5±86.50 J and 1379±244.4 J, respectively.

To isolate water as a potential driving factor of energy delivery, CRF probes were run under both CRF and SRF clinical parameters, but the water circulation function was turned off. The energy output was significantly reduced when the water circulation was turned off (CRFA 17Ga/4 mm vs CRF no water 17Ga/4 mm: 1379±244.4 vs 454.1±134.7 J at 80°C for 90 s, and vs 308.16±53.46 J at 60°C for 150 s). CRF probes without water did not reach the energy output levels of the water-circulating conditions even with alterations in multiple independent variables.

Cooled probes induce significant axonal disruption in SNs

SNs were harvested and processed histologically. In cross-sections, SNs were evaluated following CRF and SRF ablations at 6 hours. All ablated nerve sections displayed typical thermal damage

characteristics, including coagulation of epineurial, perineurial and/or endoneurial collagen, acute axonal necrosis and axon sheath swelling. However, axon sheath swelling, displayed as an enlargement of the axon sheath by white spaces in figure 2A, was greater in nerves treated using CRF 17Ga/4 mm probes than in sham or SRF probes (18Ga/10 mm and 16Ga/10 mm). The extent and severity of the thermal injury characteristics were quantified by mean scores. Mean scores (±SD) of axonal separations, the distance between the borders of axon sheaths, was greater at 0-and 6 hours following CRF procedures (figure 2B) vs all SRF groups. More notably in figure 2C, mean scores (±SD) of axon sheath swelling showed CRF large probes induced significantly more swelling in SNs than SRF probes at all time points (CRFA 17Ga/4 mm vs SRF 18Ga/10 mm: 0.63±0.15 vs 0.20±0.09 and vs SRF 16Ga/10 mm 0.25±0.10 at 0 hours) (CRFA 17Ga/4 mm vs SRF 18Ga/10 mm: 1.60±0.27 vs 0.53±0.13 and vs SRF 16Ga/10 mm 0.60±0.13 at 6 hours).

In longitudinal sections with CRF probe, 17Ga/4 mm, SNs were stained with H&E and three zones of lesions were observed (figure 3: bottom panel). These zones were represented as mild cell damage (pink zone), sandwiched between severe cellular damage (purple zones). In contrast, in nerves ablated using large SRF probes (18Ga/10 mm and 16Ga/10 mm), only one elongated region of severe thermal damage, depicted as a dark purple zone, was observed (figure 3). The average lesion size expressed as a proportion of exposed tip length was significantly smaller with SRF probes compared with CRF probes (CRF 17Ga/4 mm 2.110±0.34 mm vs SRF 18Ga/10 mm 0.68±0.264; vs SRF16Ga/10 mm 1.001±0.07) (figure 4).

To examine the true effect of probe size, we turned off the water-circulating feature during the CRF procedure. CRF lesions with no water displayed a loss in CRF's three zones, mirroring the single-zoned SRF lesions. Additionally, CRF lesion length was significantly reduced (CRF 17Ga/4 mm 2.110±0.34 mm vs CRF 17Ga/4 mm (no water) 1.135±0.6263).

SRFA and CRFA produced analogous lesion microenvironments

The activated immune response (6 hours) following thermal ablations with large RF probes (SRF 18Ga/10 mm, SRF 16Ga/10 mm and CRF 17Ga/4 mm) was assessed via IHC staining. Findings from the IHC staining in this study were qualitative changes, described and scored as absent, minimal, mild, moderate, marked or severe (online supplemental figure 1). Notably, immunolabeling exhibited expected patterns consistent with thermal lesions following RF procedures with standard and cooled technologies at 0 and 6 hours.

As expected for thermal lesions, SRF-ablated zones exhibited moderate staining of MBP with mild myelin PLP immunolabeling indicative of myelin sheath swelling. Staining of myelin markers in CRF ablation samples closely resembled the SRF samples; however, the cooled regions and sections without lesions captured a lower intensity of myelin sheath staining.

NEFH, an axon marker, exhibited strong intensities and uniform labeling in the non-ablated sections of nerves for both RF technologies. In ablated samples, NEFH immunolabeling was absent due to areas of swollen, fragmented and distorted axons with irregular borders. A slight difference in staining was observed between ablated and cooled areas of CRF samples; cooled areas exhibited increased NEFH staining in this myelin sheath area, as described above.

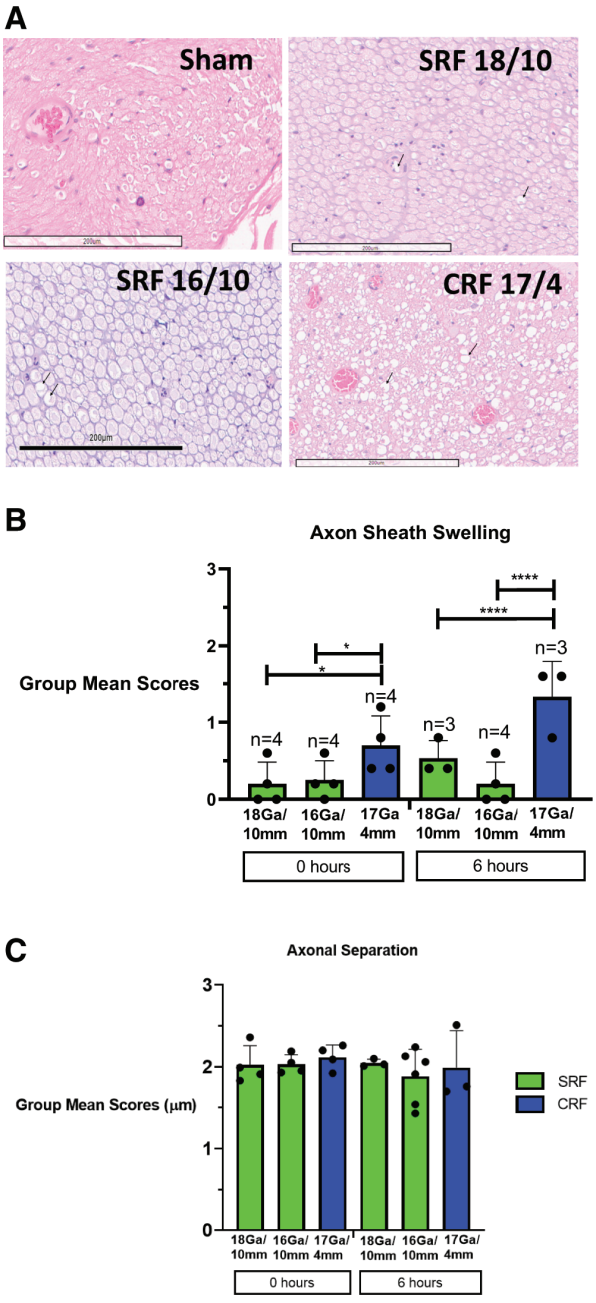

Figure 2 Cooled probes feature significantly more axonal disruption than standard large probes. (A) Representative cross-sectional images from rat sciatic nerves treated with thermal ablation arranged from least damage (sham, control) to greatest cellular damage including axonal/axon sheath swelling (CRF 17Ga/4mm) depicted in images as clear spaces ('clear spaces' indicated by black arrows). Both SRF 18Ga/10mm or SRF 16Ga/10mm treatment showed only some axon swelling. Bars: 200–300µm (B) CRF treatments induced significantly more axon sheath swelling than SRF treated groups at 0- and 6-hour time points. (C) Axon separation is greater in CRF treatments than SRF treatments at 0- and 6-hour time points. Histopathology and mean scores were measured by a histopathologist who was blinded to the treatment groups. Bars represent mean±SD for n=3-6 per group per treatment; Blue bars for cooled RF groups and green for standard RF groups. Statistical significance was indicated as *P<0.05, **P<0.01, ****P<0.0001 for n=3–4 per group per treatment. CRF, cooled radiofrequency; RF, radiofrequency; SRF, standard radiofrequency.

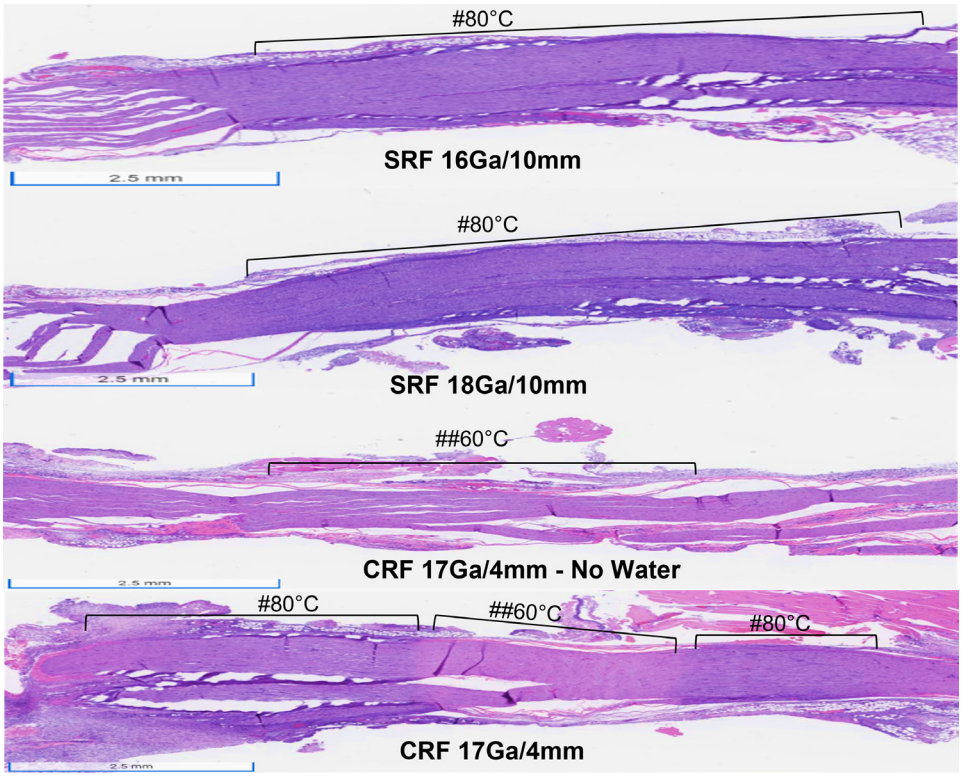

Figure 3 Sciatic nerve lesions created with RF water-circulating probes resulted in three distinct lesion zones, which mimics the predicted thermal profile. Representative H&E-stained longitudinal, sciatic nerve sections following RF ablation with SRF probes (18Ga/10mm and 16Ga/10mm) and CRF probes (17Ga/4mm) with and without internal water circulation (n=3-4). # regions correspond to 80°C thermal damage (purple); ## regions correspond to 60°C thermal damage (dark pink). CRF, cooled radiofrequency; RF, radiofrequency; SRF, standard radiofrequency.

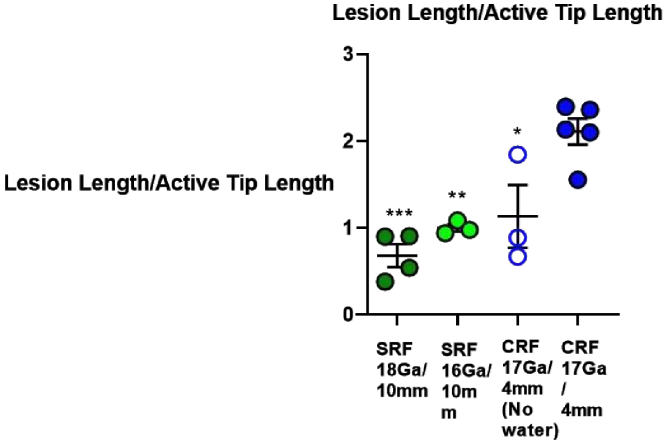

Figure 4 Water-circulating feature effects lesion length following RF ablations with different probe sizes. Lesion lengths for all treatment groups were measured by a histopathologist who was blinded to the treatment groups. Data was depicted as a proportion, lesion length (mm) divided by active tip length (mm). CRF lesion lengths relative to probe size were significantly longer than non-water circulating groups; SRF probes (18Ga/10mm and 16Ga/10mm) and CRF 17Ga/4mm without water feature (n=3-5). 'CRF 17Ga/4mm (no water)' denotes a cooled probe delivering RF energy without the water circulation through the probe. Points represent mean±SD. Statistical significance was indicated as *P<0.05, **P<0.01, ***P<0.001 for n=3–5 per group per treatment. CRF, cooled radiofrequency; RF, radiofrequency; SRF, standard radiofrequency.

S100a staining is typically observed in Schwann cell immune activation[20] in the cytoplasm surrounding myelin sheaths and scattered along the axonal profiles throughout the fascicle. In non-ablated areas, S100a intensity was minimal, while increased intensity and Schwann cell hypertrophy were observed in ablated regions in CRF and SRF samples. Similarly, S100a-immunolabeling and NEFH were less intense in the cooled areas than ablation zones in CRF samples.

CD11b-immunolabeled inflammatory cells were absent in non-ablated nerve sections. In ablated samples, very rare infiltration of individualized CD11b-labeled cells were present within the nerve fascicle. There was not a substantial difference in the inflammatory response observed among SRF or CRF ablations at the 6-hour time point, although soft tissue inflammatory cells were identified in many samples.

SRF and CRF large probes induced immediate reduction in nerve function

EMG activity (M responses) was evoked by SN stimulation before and immediately following the sham or RF procedure with SRF and CRF probes (SRF 18Ga/10 mm, SRF 16Ga/10 mm and CRF 17Ga/4 mm). For all rats in this study, the amplitudes of evoked M responses were expressed as a ratio of pre-ablation to post-ablation activity. Figure 5 shows a significant reduction in recorded M-responses (mean difference) with SRF probes 18Ga/10 mm (−1.9), 16Ga/10 mm (−2.4) and CRF probe 17Ga/4 mm (−3.2). A similar degree of reduction in nerve function were found between the treatment groups.

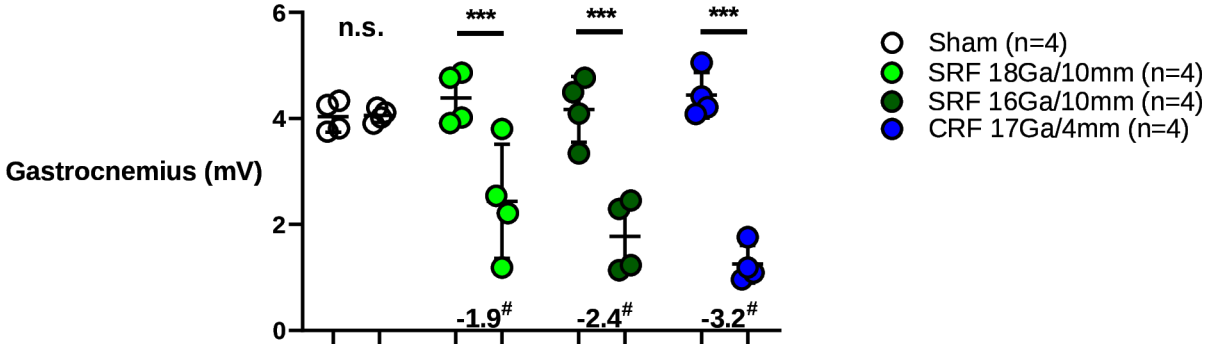

Figure 5 Amplitudes of post-procedure M-responses were significantly depressed following both SRF and CRF large probe ablations. Average gastrocnemius muscle electromyographic (EMG) amplitude was recorded for different size SRF and CRF probes prior to and immediately after ablation of the sciatic nerve. Each point represents the mean±SD. # Mean difference of post-procedure and pre-procedure EMG recordings. Statistical significance was indicated as ***P<0.001 for n=4 per group per treatment. CRF, cooled radiofrequency; RF, radiofrequency; SRF, standard radiofrequency.

DISCUSSION

Our study aimed to address the importance of probe design features for RF-desired tissue damage. We examined a wider range of commercially available probe sizes to compare structural and functional outcomes of SRF and CRF technologies. Previous investigations demonstrated that CRF delivers more energy to target tissues, resulting in longer nerve blockades and larger lesion zones than SRF.[10] Building on the literature findings, we found that CRF's water-circulating feature is a primary driver of energy delivery and structural outcomes, more than probe size.

This study suggests that there are some key factors to consider when using different RF technologies. Specifically, the CRF's system water-circulating feature can result in greater thermal energy delivery than SRF, despite larger probe sizes. Our results demonstrated that RF energy output increased as the exposed tip length and gauge of probes increased for both technologies. In a head-to-head assessment, we discovered that CRF probes delivered more energy compared with the SRF probes, despite smaller exposed tip length and width. Our findings also indicate that energy deposition for cooled probes is primarily influenced by the internally cooled, water-circulating fluid. This finding was supported when the water-circulation feature was turned off during the CRF procedure, which led to a significant reduction in energy output.

As per Sunderland's classification, third-degree peripheral nerve injury occurs as a result of neural ablations that disrupt the myelin, axon and endoneurium, while leaving the fascicular arrangement, perineurium and epineurium intact.[19 21 22] In our current study using different RF probe sizes, we observed multiple ablation zones with CRF and only one continuous ablation zone in SRF-treated SNs. The three distinct ablation zones found in CRF ablated nerves correspond to the predicted thermal profiles observed in ex vivo[9] and in vivo[10] models and should be considered a hallmark feature for all CRF probe sizes.

Moreover, the water-circulating feature of CRF probes altered biophysical characteristics of the lesion. When the water feature was turned off, the multiple ablation zones disappeared, and we observed one continuous lesion comparable to nerves after SRF treatment. Additionally, CRF's lesion length was two times the size of the active tip length but was significantly reduced without water circulation. These findings provide valuable insights into RF because larger lesions improve the odds of successful nerve targeting and increase the chances of interventional success following RF procedures.[23]

Neural ablation methods like RFA have proven to be an effective method for pain relief. However, if nerve functional recovery is poor, the innate-immune response is typically inefficient in its response to the injury.[24] MRI observed the presence of lesions for up to 1-week post-SRF and 2 weeks post-CRF ablations in vivo,[10] but to our knowledge, this is the first study to analyse the lesion microenvironment of SNs post-ablation for both RF technologies. In this study, we assessed immune cells and the structural integrity of the lesion microenvironment for SRF and CRF lesions within 6 hours post-ablation. Although differences in cellular events were not observed, we cannot rule out what others might find using other methods. Highlighting the impact of nerve repair on nerve functional recovery with respect to cellular response, timing and magnitude may lead to future investigations to clarify clinical durability differences between RF technologies.

Functional data showed similar reductions in nerve conduction after using RF large probes (SRF 16Ga/10 mm; CRF 17Ga/4 mm). In our previous study with smaller probes, we illustrated that SRF (22Ga/5 mm) had a larger M-response than CRFA (17Ga/2 mm) in as early as 1 week.[10] In subsequent pilot studies, our group uncovered limited nerve recovery in rat SN models when assessing long-term functional outcomes (~12 weeks) with large probes. We hypothesized that the large RF probes delivered an excessive amount of energy for the size of the rodent's nerve and the surrounding tissue to withstand. Therefore, our lab suggests using larger animal models, more akin to humans, to assess long-term, large probe functional outcomes. Our future goal is to develop a large animal model with complex disease processes such as osteoarthritis to target sensory nerve function directly with large RF probes and investigate biological factors that influence functional outcomes.

The results of this study may not extend to all types of nerves. A limitation of the study included our assumption that mixed or motor nerve repair is comparable to sensory nerve restoration. The SN model, a mixed nerve, is an established model for peripheral nerve injury,[18 25 26] and comparable in size to the sensory nerves typically targeted for knee ablations.[27] However, similar studies of RF ablation in other types of nerves used in clinical practice would be laudable for further translation of these results and should be the object of future investigations.

Altogether, we compared multiple sized, commercially available CRF and SRF probes head-to-head. We highlighted the impact of water circulation in probe design and its effect on lesion characteristics. The water circulation system allows CRF to lower temperatures at the electrode–tissue interface to deliver significantly more energy in tissue than SRF, without creating desiccation. As a result, CRF water-circulating technology drives distal lesion lengths and greater axonal damage than SRF. Our results provide novel evidence that the water-circulating feature of CRF probes is a primary influence in

lesion characteristic differences between RF technologies and cannot be surpassed by an increase in probe size alone. This data may shed light on CRF's sustained clinical benefits of pain relief and function in patients.

X Maxim S Eckmann @eckmann_max

Contributors AC served as the guarantor. GA, RY and JM collected data. MSE, DAP, AWE, AW and RW served as scientific advisors.

Funding The authors have not declared a specific grant for this research from any funding agency in the public, commercial or not-for-profit sectors.

Competing interests AC was employed by Avanos Medical as a Research Scientist. GA was employed by Avanos Medical as a Research Scientist. RY was employed by Avanos Medical as a Research Scientist. JM was employed by Avanos Medical as a Senior Research Scientist. ME reports personal fees from Avanos and Abbott; receives funding outside submitted from SPR Therapeutics. DP reports personal fees from Avanos, Boston Scientific, Medtronic, Nevro, and SI Bone. Pain Diagnostics and Interventional Care has received research support from Avanos, Boston Scientific, Medtronic, Nevro, Stimgenics, and Abbott. AWE reports personal fees from Avanos Medical Science Advisory Board, outside the submitted work. AVW was employed by Avanos Medical as a Manager. RW was employed by Avanos Medical as an Associate Director.

Patient consent for publication Not applicable.

Ethics approval Not applicable.

Provenance and peer review Not commissioned; externally peer reviewed.

Data availability statement All data relevant to the study are included in the article or uploaded as supplementary information.

ORCID iDs
Alyssa Cobbs http://orcid.org/0009-0003-1060-3577
David Anthony Provenzano http://orcid.org/0000-0002-2147-3523

REFERENCES

1 Jamison DE, Cohen SP. Radiofrequency techniques to treat chronic knee pain: a comprehensive review of anatomy, effectiveness, treatment parameters, and patient selection. *J Pain Res* 2018;11:1879–88.
2 Cheng J, Pope JE, Dalton JE, *et al*. Comparative outcomes of cooled versus traditional radiofrequency ablation of the lateral branches for sacroiliac joint pain. *Clin J Pain* 2013;29:132–7.
3 Leggett LE, Soril LJJ, Lorenzetti DL, *et al*. Radiofrequency ablation for chronic low back pain: a systematic review of randomized controlled trials. *Pain Res Manag* 2014;19:e146–53.
4 Kallas ON, Nezami N, Singer AD, *et al*. Cooled radiofrequency ablation for chronic joint pain secondary to hip and shoulder osteoarthritis. *Radiographics* 2022;42:594–608.
5 Organ LW. Electrophysiologic principles of radiofrequency lesion making. *Appl Neurophysiol* 1976;39:69–76.
6 Cosman ER, Dolensky JR, Hoffman RA. Factors that affect radiofrequency heat lesion size. *Pain Med* 2014;15:2020–36.
7 Nath S, DiMarco JP, Haines DE. Basic aspects of radiofrequency catheter ablation. *J Cardiovasc Electrophysiol* 1994;5:863–76.
8 Haines DE, Verow AF. Observations on electrode-tissue interface temperature and effect on electrical impedance during radiofrequency ablation of ventricular myocardium. *Circulation* 1990;82:1034–8.
9 Cedeno DL, Vallejo A, Kelley CA, *et al*. Comparisons of lesion volumes and shapes produced by a radiofrequency system with a cooled, a protruding, or a monopolar probe. *Pain Physician* 2017;20:E915–22.
10 Zachariah C, Mayeux J, Alas G, *et al*. Physiological and functional responses of water-cooled versus traditional radiofrequency ablation of peripheral nerves in rats. *Reg Anesth Pain Med* 2020;45:792–8.
11 Choi W-J, Hwang S-J, Song J-G, *et al*. Radiofrequency treatment relieves chronic knee osteoarthritis pain: a double-blind randomized controlled trial. *Pain* 2011;152:481–7.
12 Santana Pineda MM, Vanlinthout LE, Moreno Martín A, *et al*. Analgesic effect and functional improvement caused by radiofrequency treatment of genicular nerves in patients with advanced osteoarthritis of the knee until 1 year following treatment. *Reg Anesth Pain Med* 2017;42:62–8.
13 Kirdemir P, Çatav S, Alkaya Solmaz F. The Genicular nerve: radiofrequency lesion application for chronic knee pain. *Turk J Med Sci* 2017;47:268–72.
14 Hunter C, Davis T, Loudermilk E, *et al*. Cooled radiofrequency ablation treatment of the genicular nerves in the treatment of osteoarthritic knee pain: 18- and 24-month results. *Pain Pract* 2020;20:238–46.
15 Davis T, Loudermilk E, DePalma M, *et al*. Twelve-month analgesia and rescue, by cooled radiofrequency ablation treatment of osteoarthritic knee pain: results from a prospective, multicenter, randomized, cross-over trial. *Reg Anesth Pain Med* 2019;44:499–506.
16 Chen AF, Khalouf F, Zora K, *et al*. Cooled radiofrequency ablation provides extended clinical utility in the management of knee osteoarthritis: 12-month results from a prospective, multi-center, randomized, cross-over trial comparing cooled radiofrequency ablation to a single hyaluronic acid injection. *BMC Musculoskelet Disord* 2020;21:363.
17 Boeltz T, Ireland M, Mathis K, *et al*. Effects of treadmill training on functional recovery following peripheral nerve injury in rats. *J Neurophysiol* 2013;109:2645–57.
18 Cannoy J, Crowley S, Jarratt A, *et al*. Upslope treadmill exercise enhances motor axon regeneration but not functional recovery following peripheral nerve injury. *J Neurophysiol* 2016;116:1408–17.
19 Choi EJ, Choi YM, Jang EJ, *et al*. Neural ablation and regeneration in pain practice. *Korean J Pain* 2016;29:3–11.
20 Chernov AV, Dolkas J, Hoang K, *et al*. The calcium-binding proteins S100A8 and S100A9 initiate the early inflammatory program in injured peripheral nerves. *J Biol Chem* 2015;290:11771–84.
21 Sunderland S. A classification of peripheral nerve injuries producing loss of function. *Brain* 1951;74:491–516.
22 Campbell WW. Evaluation and management of peripheral nerve injury. *Clin Neurophysiol* 2008;119:1951–65.
23 Desai MJ, Safriel Y. MRI for in vivo analysis of ablation zones formed by cooled radiofrequency Nneurotomy to treat chronic joint pain across multiple axial spine sites. *J Pain Res* 2022;15:423–30.
24 Rotshenker S. Wallerian degeneration: the innate-immune response to traumatic nerve injury. *J Neuroinflammation* 2011;8:109.
25 English AW, Wilhelm JC, Sabatier MJ. Enhancing recovery from peripheral nerve injury using treadmill training. *Ann Anat* 2011;193:354–61.
26 Chen Y, Pan Z, Meng F, *et al*. Assessment of rat sciatic nerve using diffusion-tensor imaging with readout-segmented echo planar imaging. *Front Neurosci* 2022;16:938674.
27 Manzano D, Jimenez F, Blasi M. Ultrasound-guided pain interventions in the knee region. *Techniques in Regional Anesthesia and Pain Management* 2013;17:131–9.